
DIRECT NUMERICAL SIMULATION OF A TURBULENT BOUNDARY LAYER ON A FLAT PLATE USING SYNTHETIC TURBULENCE GENERATION

James Wright

Ann and H. J. Smead Aerospace Engineering Sciences
University of Colorado Boulder
Boulder, CO 80309
james.wrightiii@colorado.edu

Riccardo Balin

Ann and H. J. Smead Aerospace Engineering Sciences
University of Colorado Boulder
Boulder, CO 80309
riccardo.balin@colorado.edu

John W. Patterson

Ann and H. J. Smead Aerospace Engineering Sciences
University of Colorado Boulder
Boulder, CO 80309
jopa@colorado.edu

John A. Evans

Ann and H. J. Smead Aerospace Engineering Sciences
University of Colorado Boulder
Boulder, CO 80309
john.a.evans@colorado.edu

Kenneth E. Jansen

Ann and H. J. Smead Aerospace Engineering Sciences
University of Colorado Boulder
Boulder, CO 80309
jansenke@colorado.edu

December 22, 2024

ABSTRACT

The turbulent boundary layer over a flat plate is computed by direct numerical simulation (DNS) of the incompressible Navier-Stokes equations as a test bed for a synthetic turbulence generator (STG) inflow boundary condition. The inlet momentum thickness Reynolds number is approximately 1,000. The study provides validation of the ability of the STG to develop accurate turbulence in 5 to 7 boundary layer thicknesses downstream of the boundary condition. Moreover, the grid resolution required for both the development region and the downstream flow is investigated when using a stabilized finite element method.

1 Introduction

Direct numerical simulation (DNS) resolves all of the turbulent scales of motion leaving none to be modeled on the interior of the domain. The only modeling approximation is introduced through its need for boundary conditions. For some flow conditions, periodicity can be employed though this introduces a largest length scale that may influence the solution. For spatially developing flows, the influence of the boundary condition is felt more directly through the prescription of an unsteady inflow boundary condition. This paper studies the influence of a particular STG boundary condition proposed in [1].

This paper is organized as follows. Section 2 describes in detail the flow problem chosen and the numerical approach taken to obtain a solution with DNS. Section 3 presents and discusses the results obtained from the DNS. Finally, Section 4 offers some concluding remarks.

2 Numerical Setup

2.1 Problem Definition

The flow computed in this study is the turbulent boundary layer over a zero pressure gradient flat plate. The momentum thickness Reynolds number at the inflow is $Re_\theta = 970$, which is typical of DNS of more complex flows [2]. While far from the highest Re simulated [3, 4, 5], the goal here is different. By choosing a modest size simulation, a careful study of the inflow boundary condition and other aspects of the simulation, such as numerical method (and associated dissipation) and the grid resolution requirements, can be compared.

2.2 Solution Approach

At the inflow, the STG method of [1] was selected in order to provide unsteady and spatially varying velocity fluctuations into the domain. This method has been shown to produce realistic turbulence a short distance downstream of the inlet for both wall-modeled LES and DNS [1, 6]. According to this approach, velocity fluctuations are first computed from a superposition of spatiotemporal Fourier modes with random amplitudes and phases. These are then scaled by prescribed profiles of the time-averaged Reynolds stresses in order to obtain the desired second order moments and thus introduce synthetic scales with both anisotropy and inhomogeneity. The fluctuations are finally added to a known mean velocity profile to obtain a time and spatially varying boundary condition.

While the original concept of STG dates back to [7], more detail on the history, development, and analysis of the STG method can be found in [1] and in [8]. Here we summarize the equations and description from [8].

$$u'_i = a_{ij} 2\sqrt{\frac{3}{2}} \sum_{n=1}^N \sqrt{q^n} \sigma_j^n \cos(\kappa^n d_l^n \hat{x}_l + \psi^n) \quad (1)$$

$$\begin{aligned} \hat{x}_i &\equiv \{(x_1 - U_0 t') \max(\kappa_e^{min}/\kappa^n, 0.1), x_2, x_3\} & \sigma_j^n d_j^n &= 0 & a_{ik} a_{jk} &= R_{ij} \\ q^n &\equiv \int_{\kappa^{n-1}}^{\kappa^n} E(\kappa^n) d\kappa / \int_0^\infty E(\kappa^n) d\kappa & \sigma^n &= \sigma^n(\theta^n, \phi^n) \\ E(\kappa^n) &= (\kappa^n/\kappa_e)^4 f_\eta f_{cut} [1 + 2.4(\kappa^n/\kappa_e)^2]^{-17/6} & d_i^n &= d_i^n(\theta^n, \phi^n, \eta^n) \end{aligned}$$

Einstein summation notation has been adopted when the contraction is between spatial dimensions (subscripts) while a sum is written for Fourier components (superscripts) since they are often repeated more than twice. The terms θ^n , ϕ^n , η^n , and ψ^n are sets of random variables defined by their probability density functions and intervals: $f_\theta = \sin(\theta)/2$; $\theta \in [0, \pi]$, $f_{\phi, \eta, \psi} = \pi/2$; $\{\phi, \eta, \psi\} \in [0, 2\pi)$. The two random sets of spherical angles θ^n and ϕ^n cause the set of unit vectors, σ_j^n , to be uniformly distributed on a unit sphere. Imposing a divergence-free velocity ($\sigma_j^n d_j^n = 0$ as verified in [9]) together with the requirement that d_j^n be uniformly distributed on a unit sphere leaves d_j^n a function of σ_j^n 's dependent variables (θ, ϕ) and the angle η in the plane normal to σ_j^n . The random angles, radial lengths, and defined intensities are wave modes that have been mapped to wave space from a pseudo isotropic turbulence via the spatial Fourier transform. Note, the definition of \hat{x}_i provides a means to slide through this pseudo turbulence domain by a spatial coordinate that progresses at the inflow bulk speed, U_0 , naturally accounting for bulk convection. The second argument of the max is due to [10]. Definitions for κ_e^{min} , f_η , f_{cut} , $k_e(x_i)$ match those given in [1] where they were chosen to adjust the spectrum (eddy size and anisotropy) to accurately account for proximity to solid boundaries. Further, their approach of defining a_{ij} through a Cholesky decomposition of the Reynolds stress, R_{ij} , is adopted.

The mean velocity and Reynolds stress profiles for the flow analyzed here were obtained from Case C of the DNS study of [11] at $Re_\theta = 1,300$ and rescaled to the lower $Re_\theta = 970$ using the relations in [12]. Though it seems intuitive that normal stress profiles obtained directly from the DNS would be the best choice in order to inject synthetic scales with the correct anisotropy, in our experience and that of colleagues isotropic normal stress profiles perform better for this STG method. These are computed from the Reynolds shear stress as outlined in Eq. 2 in a similar manner to what would be performed with the solution of a RANS simulation with the Spalart-Allmaras one-equation model [13]. Note that k^{mod} is the modeled turbulent kinetic energy and $C_\mu = 0.09$.

$$k^{mod} = \frac{-\overline{u'v'}}{C_\mu} \quad \overline{u'u'} = \frac{2}{3} k^{mod} = \overline{v'v'} = \overline{w'w'} \quad (2)$$

Other boundary conditions of the DNS were as follows. The plate was treated as a no-slip wall with zero velocity. The top surface was tilted slightly downward so that it could be treated like the outflow where weak enforcement of zero pressure was applied along with zero traction. At the inflow and outflow, the top boundary was located $21\delta_{in}$ and $20\delta_{in}$ above the flat plate, respectively. The outflow was located $27\delta_{in}$ downstream of the inflow where weak enforcement of zero pressure and traction were also applied. Effects from this boundary condition on the interior domain were contained within a streamwise distance of one local boundary layer thickness and thus did not affect the upstream solution. The spanwise period was set to $3\delta_{in}$ with periodicity enforced.

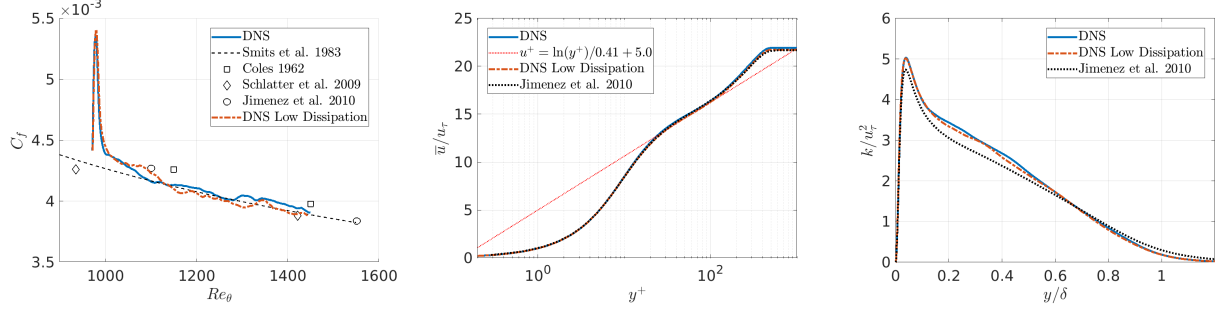


Figure 1: Left: skin friction coefficient for a zero pressure gradient flat plate DNS using STG as an inflow boundary condition. Center and right: streamwise velocity and turbulent kinetic energy profiles, respectively, at $Re_\theta = 1, 100$ for the ZPG DNS.

The grid for the DNS was designed with spacing $\Delta x^+ = 15$, $\Delta z^+ = 6$, $\Delta y_1^+ = 0.1$, and $\Delta y_{\max}^+ = 10$, where the inflow friction velocity was used for the non-dimensionalization. This resulted in a total of 31 million points. The simulations were integrated for at least five domain flow-through times and were deemed statistically stationary by looking at various sub-windows of the total accumulated time average.

2.3 Flow Solver

The Parallel-Hierarchic-Adaptive-Stabilized-Transient-Analysis (PHASTA) flow-solver was used for all simulations presented in this work. PHASTA uses a stabilized, semi-discrete finite element method to solve either the compressible or incompressible Navier-Stokes equations plus any additional set of scalar equations for turbulence modeling. While high-order hierarchical bases of polynomials are available, tri-linear hexahedral elements were selected for these simulations resulting in second order accuracy. Stabilization is performed with the streamline upwind/Petrov-Galerkin (SUPG) method [14]. Time integration is performed with the fully implicit, second-order accurate generalized- α method [15]. These high-fidelity, massively parallel computations could be performed in a reasonable time frame due to the strong scalability of PHASTA, which has been demonstrated in [16]. The accuracy of DNS with PHASTA has been shown for a channel flow in [17], in which tri-linear hexahedral elements were also used. Note finally that the incompressible branch of the solver was selected for this work due to the low Mach number of the flow.

3 Results

The skin friction coefficient computed from the flat plate ZPG DNS is shown by the solid curve (the dot-dash curve is discussed later in this section) in the left panel of Fig. 1 along with data from other DNS and experiments [18, 3, 19, 4]. After an expected initial spike immediately downstream of the STG inflow caused by the development of the correct near-wall turbulent structures, the C_f quickly drops and good agreement with the validation data is obtained. Figure 1 also shows the time-averaged streamwise velocity and turbulent kinetic energy profiles at $Re_\theta = 1, 100$ for the simulation producing the solid C_f curve. The data from the DNS of [4] at the same Re_θ is included for reference. Note that this value of Reynolds number corresponds to a distance of $7\delta_{\text{in}}$ downstream of the inlet, therefore these plots are evaluating the effectiveness of the method to quickly produce realistic turbulence. The velocity profile agrees very well with the logarithmic law and with the other DNS, and similarly the turbulent kinetic energy shows good agreement with the data. This is in spite of a fairly different turbulent kinetic energy profile being prescribed at the inflow (see Eq. 2), indicating the formation of the correct near-wall turbulence.

As an additional preliminary study, the effects of numerical dissipation were investigated on the same ZPG flat plate DNS used for testing of the STG inflow boundary condition. Numerical dissipation in PHASTA can be changed by acting on the SUPG stabilization operator [14], which affects the spatial dissipation, and the ρ_∞ parameter of the generalized- α time integrator [15]. The dashed curves in Fig. 1 show the results obtained with a reduction in both spatial and temporal dissipation by a factor of two relative to the solid curve. Differences between the skin friction predictions are 2% or less and within the scatter due to lack of full convergence of the statistics. Differences in the velocity and turbulent kinetic energy are also negligible. Consequently, the effects of numerical dissipation at this level of resolution were considered minimal.

4 Conclusions

Direct numerical simulation was performed of the turbulent boundary layer over a short flat plate utilizing an STG inflow boundary condition. The domain was chosen to be as short as feasible to test the development length of this boundary

condition – how many boundary layer thicknesses are required to reproduce an equilibrium turbulent boundary layer – as measured by agreement in skin friction coefficient, streamwise velocity, turbulent kinetic energy, and Reynolds shear stress profiles with previous numerical and experimental studies. A development length of 5-7 boundary layer thicknesses was adequate to match validation data to within 2%. Furthermore, this result was shown to be insensitive to stabilization parameters in the stabilized finite element method used indicating that stream-wise spacing of 15 plus units, span-wise spacing of 6 plus units, and a maximum wall-normal spacing of 10 plus units is adequate for this flow when discretized with structured tri-linear hexahedra.

Acknowledgements

This work was supported by the National Science Foundation, Chemical, Bioengineering, Environmental and Transport Systems grant CBET-1710670 and by the National Aeronautics and Space Administration, Transformational Tools and Technologies grant 80NSSC18M0147, both to the University of Colorado Boulder. Computational resources were utilized at the NASA High-End Computing (HEC) Program through the NASA Advanced Supercomputing (NAS) Division at Ames Research Center and at the Argonne Leadership Computing Facility (ALCF), which is a DOE Office of Science User Facility supported under Contract DE-AC02-06CH11357. Finally, the authors thank Drs. P.R. Spalart, and M.K. Strelets for the helpful insight and communications regarding the problem setup, the analysis of the flow, and the synthetic turbulence generation method.

References

- [1] M. L. Shur, P. R. Spalart, M. Kh. Strelets, and A. K. Travin. Synthetic turbulence generators for RANS-LES interfaces in zonal simulations of aerodynamic and aeroacoustic problems. *Flow, Turbulence and Combustion*, 93:63–92, 2014.
- [2] R. Balin, K. E. Jansen, and P. R. Spalart. Wall-modeled LES of flow over a Gaussian bump with strong pressure gradients and separation. In *AIAA AVIATION Forum*, Virtual Event, 2020.
- [3] P. Schlatter, R. Örlü, Q. Li, G. Brethouwer, J. H. M. Fransson, A. V. Johansson, P. H. Alfredsson, and D. S. Henningson. Turbulent boundary layers up to $Re_\theta = 2500$ studied through simulation and experiment. *Physics of Fluids*, 21:051702, 2009.
- [4] J. Jimenez, S. Hoyas, M. P. Simens, and Y. Mizuno. Turbulent boundary layers and channels at moderate Reynolds numbers. *Journal of Fluid Mechanics*, 657:335–360, 2010.
- [5] J. A. Sillero, J. Jimenez, and R. D. Moser. One-point statistics for turbulent wall-bounded flows at Reynolds numbers up to $\delta^+ \approx 2000$. *Physics of Fluids*, 25:105102, 2013.
- [6] P. R. Spalart, K. V. Belyaev, A. V. Garbaruk, M. L. Shur, M. Kh. Strelets, and A. K. Travin. Large-eddy and direct numerical simulations of the Bachalo-Johnson flow with shock-induced separation. *Flow, Turbulence and Combustion*, 99:865–885, 2017.
- [7] R. H. Kraichnan. Diffusion by a random velocity field. *The Physics of Fluids*, 12:22–31, 1970.
- [8] J.W. Patterson, R. Balin, and K.E. Jansen. Assessing and improving the accuracy of synthetic turbulence generation. *Journal of Fluid Mechanics – Rapids*, Accepted: 2020.
- [9] A. Smirnov, S. Shi, and I. Celik. Random flow generation technique for large eddy simulations and particle-dynamics modeling. *Journal of Fluids Engineering*, 123:359–371, 2001.
- [10] M. L. Shur. private communication, 2020.
- [11] G. N. Coleman, C. L. Rumsey, and P. R. Spalart. Numerical study of turbulent separation bubbles with varying pressure gradient and Reynolds number. *Journal of Fluid Mechanics*, 847:28–70, 2018.
- [12] T. S. Lund, X. Wu, and K. D. Squires. Generation of turbulent inflow data for spatially-developing boundary layer simulations. *Journal of Computational Physics*, 140:233–258, 1998.
- [13] P. R. Spalart and S. R. Allmaras. A one equation turbulence model for aerodynamic flows. *AIAA Journal*, 94, 1992.
- [14] Christian H. Whiting and Kenneth E. Jansen. *Stabilized Finite Element Methods For Fluid Dynamics Using A Hierarchical Basis*. PhD thesis, Rensselaer Polytechnic Institute, 1999.
- [15] Kenneth E. Jansen, Christian H. Whiting, and Gregory M. Hulbert. Generalized- α method for integrating the filtered Navier-Stokes equations with a stabilized finite element method. *Computer Methods in Applied Mechanics and Engineering*, 2000.
- [16] O. Sahni, C.D. Carothers, M.S. Shephard, and K.E. Jansen. Strong scaling analysis of an unstructured, implicit solver on massively parallel systems. *Scientific Programming*, 17:261–274, 2009.

- [17] A. V. Trofimova, A. E. Tejada-Martinez, and K.E. Jansen. Direct numerical simulation of turbulent channel flows using a stabilized finite element method. *Computers & Fluids*, 38:924–938, 2009.
- [18] D. E. Coles. The turbulent boundary layer in a compressible fluid. Technical Report R-403-PR, The Rand Corporation, 1962.
- [19] A. J. Smits, N. Matheson, and P. N. Joubert. Low-Reynolds-number turbulent boundary layers in zero and favorable pressure gradients. *Journal of Ship Research*, 27:147, 1983.